

# From Nodal Chain Semimetal To Weyl Semimetal in HfC

Rui Yu<sup>1,\*</sup>, Quansheng Wu<sup>2</sup>, Zhong Fang<sup>3,4</sup>, and Hongming Weng<sup>3,4†</sup>

<sup>1</sup> *School of Physics and Technology,*

*Wuhan University, Wuhan 430072, China*

<sup>2</sup> *Theoretical Physics and Station Q Zurich,*

*ETH Zurich, 8093 Zurich, Switzerland*

<sup>3</sup> *Beijing National Laboratory for Condensed Matter Physics,*

*and Institute of Physics, Chinese Academy of Sciences, Beijing 100190, China and*

<sup>4</sup> *Collaborative Innovation Center of Quantum Matter, Beijing 100190, China*

## Abstract

Based on first-principles calculation and effective model analysis, we propose that the WC-type HfC can host three-dimensional (3D) nodal chain semimetal state when spin-orbit coupling (SOC) is ignored. Two types of nodal rings constitute the nodal chain, which are protected by mirror reflection symmetries of a simple space group. This is remarkably distinguished from the nodal chain known in IrF<sub>4</sub> [1], where the crystal symmetry of nonsymmorphic space group with glide plane are necessary. When SOC is included, the nodal chain in WC-type HfC evolves into three types, 30 pairs of Weyl points. The surface states and the pattern of the surface Fermi arcs connecting these Weyl points are studied, which may be measured by future experiments.

---

\* [yurui1983@foxmail.com](mailto:yurui1983@foxmail.com)

† [hmweng@iphy.ac.cn](mailto:hmweng@iphy.ac.cn)

## I. INTRODUCTION

Materials with novel Fermi surface have generated significant interest in the field of solid state physics[1–5]. The symmetries of crystal give the constraints to the band structure of quasiparticles, which may lead to the quasiparticles near the Fermi energy behave like Dirac Fermions or Weyl Fermions that are first come up with in high-energy physics, or some other novel quasiparticles that have no high-energy correspondence. For example, topological nontrivial semimetals can host three- [4–6], four- [7, 8], six- [3], or eight-fold [3, 9] degeneracy bands crossing points which are protected by special crystalline symmetries on high symmetrical crystal momentum points or along high symmetry lines. The two-fold degeneracy bands crossing points, namely the Weyl points [10–14] are protected by the lattice translation symmetry without other additional crystalline symmetries. In a particular case, the bands crossing points are not discrete located in the Brillouin zone but form closed loops, which are called as the nodal line [15–17] and nodal chain semimetals [1]. Three types of nodal line semimetals have been proposed in systems with mirror reflection symmetry (type I) [18–21], or coexistence of time-reversal symmetry and space inversion symmetry (type II) [22–25], or with nonsymmorphic space group with glide plane or screw axes symmetries (type III) [1, 25]. The properties induced by these novel band structures include the exotic surface Fermi arc states [10, 26], the chiral anomaly in Dirac and Weyl semimetal states [26–28], and the drum-head like surface states proposed in nodal line and nodal chain semimetals [22, 23, 29].

In the present paper we propose that the WC-type HfC is a material that hosts a three-dimensional nodal chain in the Brillouin zone when the SOC is ignored. The nodal chain is composed of two types of nodal rings which belong to the type II nodal line structure protected by the mirror reflection symmetry in the  $k_z = 0$  and  $k_y = 0$  plane, respectively. This is remarkably distinguished from the nodal chain known in IrF<sub>4</sub> [1], which is protected by the glide plane in the nonsymmorphic space group. In our paper, the proposed nodal chain is only protected by mirror symmetries, which may happen in simple space group for spinless electronic systems, photonic and phononic crystal systems.

Similar to TaAs and ZrTe [4, 12], the SOC in HfC opens gap along the nodal chain and leads to three types of Weyl nodes pairs off the mirror planes. Due to the time-reversal and crystalline symmetries, totally there are 30 pairs of Weyl nodes. The surface states and the

patterns for the surface Fermi arcs connecting the Weyl points with different Fermi energy are studied.

## II. CRYSTAL STRUCTURE OF HfC AND METHODOLOGY

The WC-type HfC crystallizes in the hexagonal space group  $P\bar{6}m2$  (No. 187). Hf and C atoms occupy the  $1d$  ( $\frac{1}{3}, \frac{2}{3}, \frac{1}{2}$ ) and  $1a$  (0,0,0) Wyckoff positions as shown in Fig. 1 (a,b). The lattice constants are  $a=b=3.267$  Å and  $c=2.942$  Å[30]. All the results discussed in the following are from the calculations with this structure.

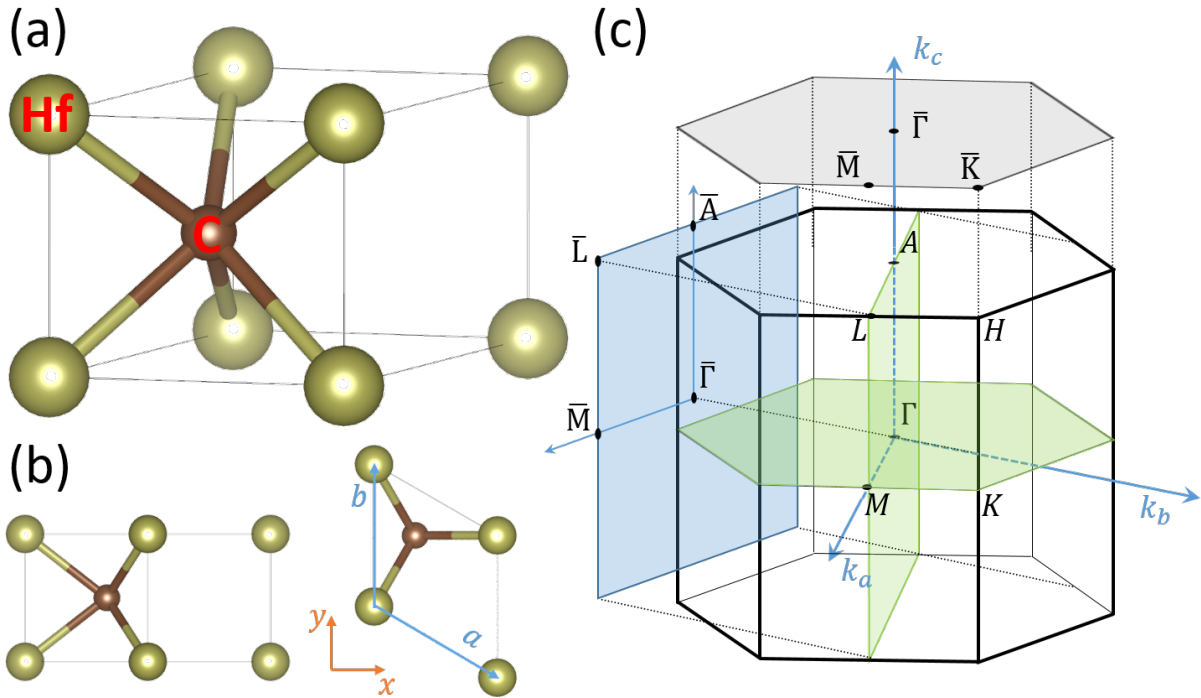


Figure 1. (Color online) (a) The primitive cell of WC-type HfC and its (b) top view and side view. Hf and C atoms occupy the  $1d$  ( $\frac{1}{3}, \frac{2}{3}, \frac{1}{2}$ ) and  $1a$  (0,0,0) Wyckoff positions. (c) The bulk Brillouin zone and its projection onto the (010) and (001) direction. The high symmetrical crystal momenta and  $k_z = 0$ ,  $k_y = 0$  mirror planes are indicated.

We perform density functional calculations by using the Vienna *ab initio* simulation package [31] with generalized gradient approximation (GGA) [32] and the projector augmented-wave method [33]. SOC is taken into account self-consistently. The surface band structures are calculated in a tight-binding scheme that projected from the bulk Bloch wave functions

based on the maximally localized Wannier functions (MLWF) [34, 35].

### III. BAND STRUCTURE OF HFC

The band structures calculated within GGA are shown in Fig. 2 (a). It clearly shows that two band-crossing-structures exist near the Fermi energy. One crosses around  $\Gamma$  point and the other one crosses around M point. The fat-band structure shows that the two crossing bands around  $\Gamma$  point are dominated by  $Hf : d_{xy}$  and  $C : p_z$  orbitals for valence band and conduction band, respectively. While the bands crossing around M point are dominated by  $Hf : d_{xz}$  and  $C : p_y$  orbitals for valence band and conduction band, respectively. The calculated Fermi surface is shown in Fig. 2 (b-c), where the surface with blue color comes from the conduction bands and the red part comes from the valence bands. Two types of ring structures exist in the Fermi surface. The first type of rings lie in the  $k_z = 0$  plane and surround the  $\Gamma$  point, the second type of rings lie in the  $k_y = 0$  plane and surround the M point. The lotus-root-like Fermi surface wraps the bands crossing loops, namely the nodal chain, as shown in Fig. 3 (b), which lie in the mirror planes that will discuss in the following text.

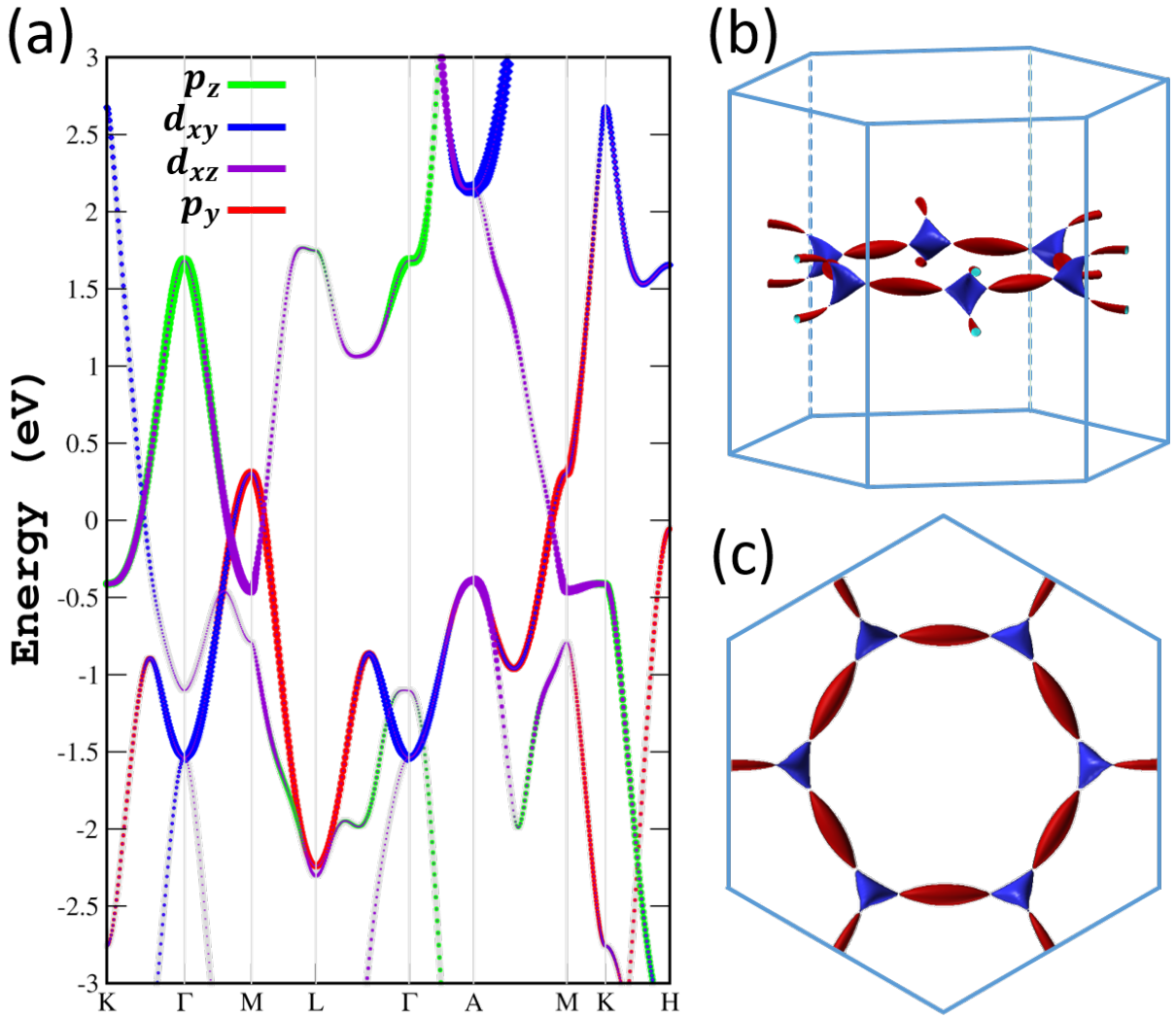


Figure 2. (Color online) (a) Band structures of WC-HfC. Two band-crossing-structures, one around  $\Gamma$  point and the other one around M point, exist near the Fermi energy. (b) side view and (c) top view of the Fermi surface of WC-HfC, which consists of electron pockets (blue) and hole pockets (red), and forms lotus-root-like structure.

#### IV. NODAL CHAIN IN HfC

We first prove the existence of nodal ring encircling the  $\Gamma$  point and lying in the  $k_z = 0$  plane. The symmetry at  $\Gamma$  point is characterized by  $D_{3h}$  symmetry group, which includes  $C_3$  rotation symmetry around  $z$  axis,  $C_2$  rotation symmetry around  $x$  axis, mirror symmetry  $M_y : (x, y, z) \rightarrow (x, -y, z)$  and  $M_z : (x, y, z) \rightarrow (x, y, -z)$  and time-reversal symmetry. A

minimal model for the two crossing bands around  $\Gamma$  point can be written as the following two-bands k-p Hamiltonian:

$$H_0^\Gamma(\mathbf{k}) = \sum_{i=x,y,z} d_i(\mathbf{k})\sigma_i, \quad (1)$$

where  $d_i(\mathbf{k})$  are real functions and vector  $\mathbf{k}$  is relative to the  $\Gamma$  point. We have ignored the term proportional to the identity matrix since it is irrelevant in the studying the band touching. The time-reversal symmetry operator is represented by  $T = K$ , where  $K$  is complex conjugate, in the absence of SOC. Time-reversal symmetry requires that

$$TH_0^\Gamma(\mathbf{k})T^{-1} = H_0^\Gamma(-\mathbf{k}), \quad (2)$$

which places an constraint on  $d_i(\mathbf{k})$  so that  $d_{x,z}(\mathbf{k})$  are even function of  $\mathbf{k}$ , while  $d_y(\mathbf{k})$  is odd function of  $\mathbf{k}$ . Now we consider the formula of  $d_z(\mathbf{k})$ , an even function of  $\mathbf{k}$ , which can be generally written as

$$d_z(\mathbf{k}) = c_0 + c_1k_x^2 + c_2k_y^2 + c_3k_z^2, \quad (3)$$

up to the second order of  $\mathbf{k}$ . The parameters  $c_i$  should be obtained by fitting with the *ab initio* calculations. The exact values for these parameters have no significant influence for the following discussions, but the sign of these parameter are the key factor for the existence of nodal rings. The sign of  $c_i$  can be obtained by checking the band dispersions as shown in Fig. 2 (a). The two bands near Fermi energy with inverted structure along  $\Gamma$ -M ( $k_x$ ) and  $\Gamma$ -K ( $k_y$ ) directions lead to  $c_0 > 0$  and  $c_{1,2} < 0$ . While the energy dispersions in the  $\Gamma$ -A ( $k_z$ ) direction is in normal order, which indicates that  $c_3 > 0$ . Due to the two considered bands ( $d_{xy}$  and  $p_z$ ) have opposite mirror eigenvalues for the  $k_z = 0$  mirror reflection,  $M_z$  may presented by  $M_z = \sigma_z$ . The mirror reflection symmetry dictates that

$$M_z H_0^\Gamma(k_x, k_y, k_z) M_z^{-1} = H_0^\Gamma(k_x, k_y, -k_z), \quad (4)$$

which lead to

$$d_{x,y}(k_x, k_y, k_z) = -d_{x,y}(k_x, k_y, -k_z), \quad (5)$$

$$d_z(k_x, k_y, k_z) = d_z(k_x, k_y, -k_z), \quad (6)$$

For the mirror symmetry in the  $k_y = 0$  plane, we may write the mirror operator  $M_y = -\sigma_y$ . This symmetry places additional constraints to  $d_i$  which reads:

$$d_{x,y}(k_x, k_y, k_z) = -d_{x,y}(k_x, -k_y, k_z), \quad (7)$$

$$d_z(k_x, k_y, k_z) = d_z(k_x, -k_y, k_z). \quad (8)$$

Equation 5, 6 indicate that on the plane  $k_z = 0$ ,  $d_{x,y}(k_x, k_y, k_z)$  are vanish. The solutions of  $d_z(k_x, k_y, 0) = 0$  determine the bands crossing points on the  $k_z = 0$  plane. Refer to the formula of  $d_z$  shown in Eq. 3, we have  $c_0 + c_1k_x^2 + c_2k_y^2 = 0$ , with  $c_0 > 0$  and  $c_{1,2} < 0$ , which leads to the bands crossing points form a circle in the  $k_x$ - $k_y$  plane, namely the nodal ring circling the  $\Gamma$  point as shown in Fig. 3 (b). In the  $k_y = 0$  plane, Eq. 7 and 8 show that  $d_{x,y}$  are vanish and the equation  $d_z(k_x, 0, k_z) = 0$  lead to  $c_0 + c_1k_x^2 + c_3k_z^2 = 0$ . Due to  $c_0, c_1 > 0$  and  $c_3 < 0$ , the solutions form a hyperbolic lines crossing the  $k_y$  axis and embracing the M, not a circle surrounding  $\Gamma$  point. These node lines are part of the nodal ring around M point that will discuss later. The last two symmetry operators,  $C_3$  and  $C_2$  rotations, which place additional symmetrical constraints to  $d_i(k_x, k_y, k_z)$ , only change the shape of the nodal rings but not affect the existence of it.

The existence of nodal ring in the  $k_y = 0$  plane encircling the M point can be proved with the similar argument. We give the details below. The little group at M point is  $C_{2v}$  which include the  $C_2$  rotation along  $x$  axis, the mirror reflection  $M_y: (x, y, z) \rightarrow (x, -y, z)$ , and the mirror reflection  $M_z: (x, y, z) \rightarrow (x, y, -z)$ . The general two bands model around the M point is give as

$$H_0^M(\mathbf{k}) = \sum_{i=x,y,z} g_i(\mathbf{k})\sigma_i, \quad (9)$$

where  $g_i(\mathbf{k})$  are real functions and vector  $\mathbf{k}$  is relative to the M point. The time-reversal symmetry leads to  $g_{x,z}(\mathbf{k})$  are even and  $g_y(\mathbf{k})$  is odd function of  $\mathbf{k}$ . Generally,  $g_z(\mathbf{k})$  may written as

$$g_z(\mathbf{k}) = a_0 + a_1k_x^2 + a_2k_y^2 + a_3k_z^2, \quad (10)$$

up to the second order of  $\mathbf{k}$ . The bands inversion along M- $\Gamma$  ( $k_x$ ) and M-L ( $k_z$ ) directions lead to  $a_0 > 0$  and  $a_{1,3} < 0$ . While in the M-K ( $k_y$ ) direction the two bands near Fermi energy are in normal order that indicates  $a_2 > 0$ . The two crossing bands near M point ( $d_{xz}$  and  $p_y$ ) with opposite mirror eigenvalues indicates that the mirror-reflection  $M_y$  may presented by  $M_y = \sigma_z$ , which lead to

$$g_{x,y}(k_x, k_y, k_z) = -g_{x,y}(k_x, -k_y, k_z), \quad (11)$$

$$g_z(k_x, k_y, k_z) = g_z(k_x, -k_y, k_z). \quad (12)$$

From Eq. 11, 12, we know that the solutions of  $g_z(k_x, 0, k_z) = a_0 + a_1 k_x^2 + a_3 k_z^2 = 0$  determine the band crossing positions, which form a close circle circling the M point in the  $k_x$ - $k_z$  plane, namely the nodal ring with green color as shown in Fig. 3. The  $C_2$  rotations, which constraints the shape of the nodal rings but keep the existence of it. The mirror symmetry on the  $k_z = 0$  plane lead to a part of nodal line embracing the  $\Gamma$  point as discussed above. Therefore, we prove that there are two type of nodal rings, the red one and the green one as shown in Fig. 3, which touch at some point along  $\Gamma$ -M direction and form a nodal chain structure in the whole BZ.

## V. WEYL NODES IN HFC

In the presence of SOC, the bands structure in Fig. 3 shows that the nodal points along  $\Gamma$ - $K$ ,  $\Gamma$ -M and M- $A$  are fully gapped. By careful check the bands structure away from the high symmetry-lines, we find that there are three types, 30 pairs, of band crossing points, namely the Weyl points, exist in the first BZ. We have located the positions and energies of all the three types of Weyl nodes as listed in Table I. All others can be found from the listed one by the time reversal and crystal symmetries. All the Weyl nodes are shown in Fig. 3 (b), where the red and blue color indicate the different chirality of them.

Weyl Point	Position ( $\text{\AA}^{-1}$ )	Energy (eV)
$W_1$	(0.411, 0.004, 0.034)	-0.047
$W_2$	(0.571, 0.017, 0.103)	0.101
$W_3$	(0.319, 0.183, 0.007)	0.147

Table I. The three nonequivalent Weyl points in the  $(k_x, k_y, k_z)$  coordinates shown in Fig. 3 (b). The position is given in units of  $\text{\AA}^{-1}$  and the energy is given in units of eV.

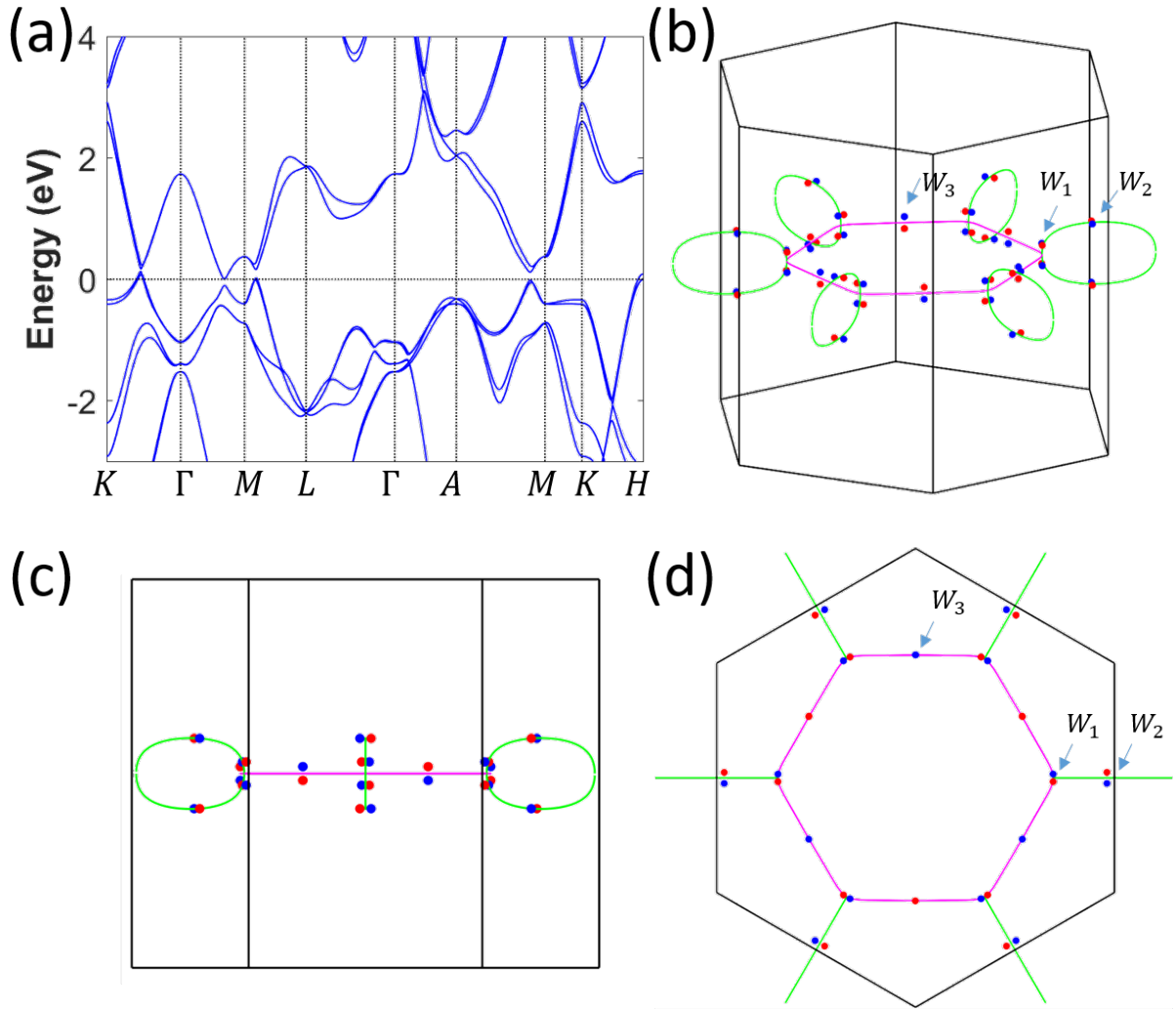


Figure 3. (Color online) (a) The band structure of HfC calculated within GGA including spin-orbit coupling (SOC). (b) 3D view of the nodal chain (in the absence of SOC) and Weyl points (with SOC) in the BZ. (c) Side view from (100) and (d) top view from (001) directions for the nodal chain and Weyl points. Once the SOC is turned on, the nodal chain are gapped and give rise to 30 pairs of Weyl points off the mirror planes.

## VI. SURFACE STATE

Based on the tight-binding model constructed by using MLWF method, we calculate the (001) surface states which are shown in Fig. 4. The projections of Weyl nodes are indicated as black points in these figures. Due to the Weyl points with left- and right-handed chirality

projected to the same point on the surface BZ, the Fermi arcs connecting with these Weyl points form complex pattern as shown in Fig. 4 with chemical potential passing through the  $W_1$ ,  $W_2$ , and  $W_3$  type Weyl nodes. The (100) surface states are shown in Fig. 5

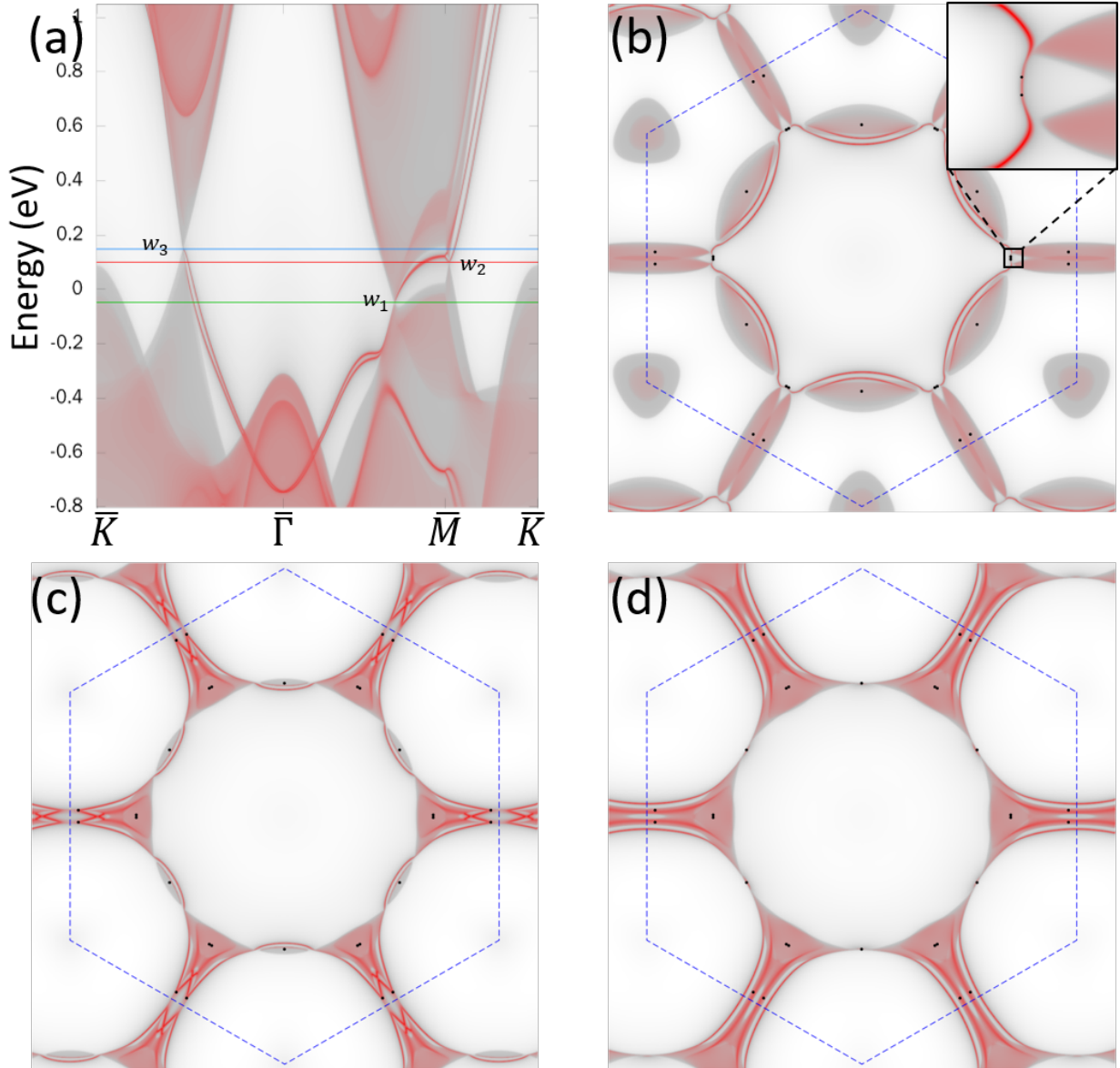


Figure 4. (Color online) (a) Surface states of HfC terminated in (001) direction. (b-d) Fermi surface of HfC (001)-surface states. Chemical potential is set at (b)  $W_1$ , (c)  $W_2$ , and (d)  $W_3$  type of Weyl point.

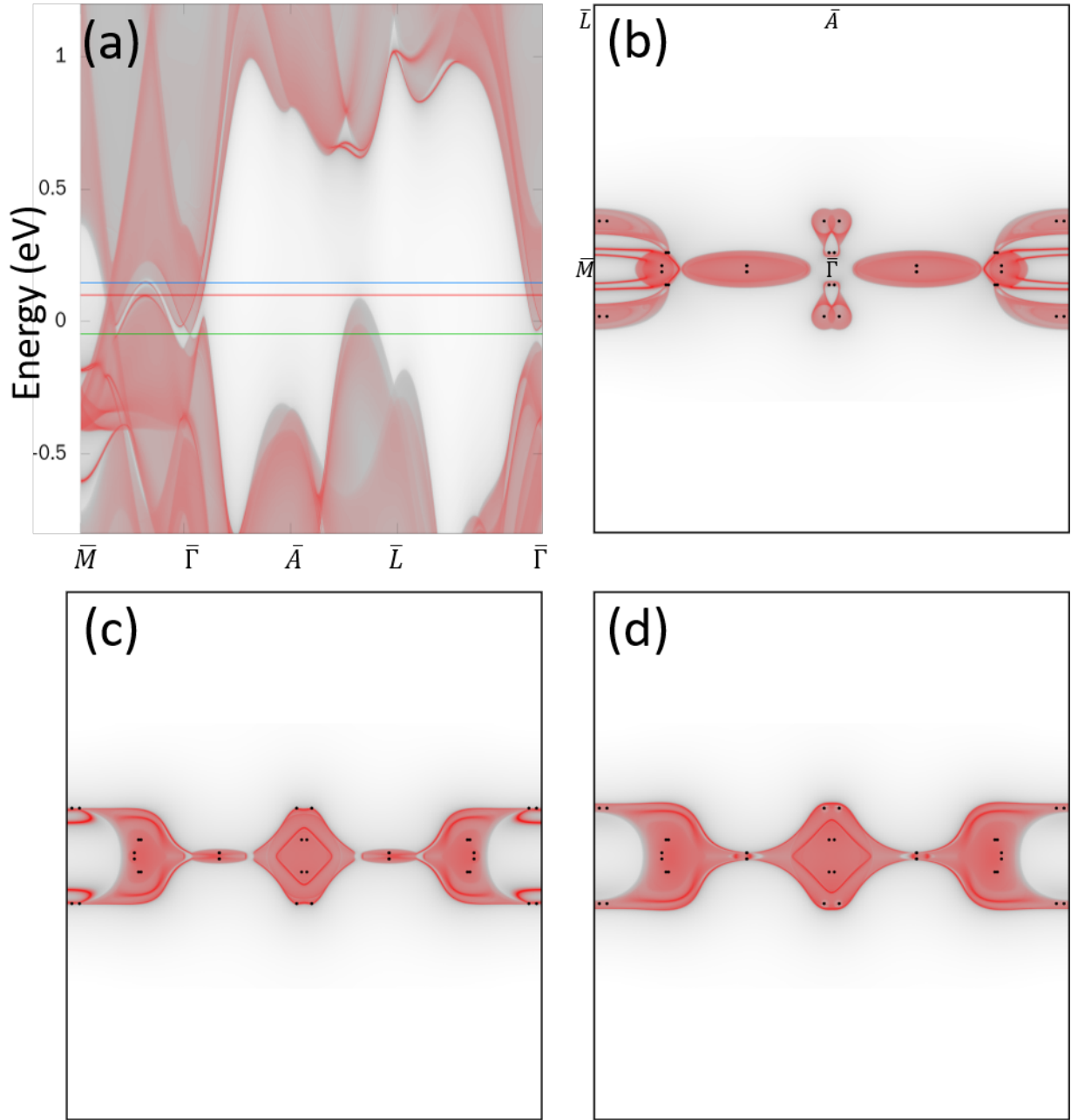


Figure 5. (Color online) (a) Surface states of HfC terminated in (100) direction. (b-d) Fermi surface of HfC (100)-surface states. Chemical potential is set at (b)  $W_1$ , (c)  $W_2$ , and (d)  $W_3$  type of Weyl point.

## VII. CONCLUSIONS

In this paper we report the nodal chain structure in WC-type HfC without spin orbit coupling. Based on first principle calculation and model analysis we confirm that two nodal rings circling the  $\Gamma$  and M points, respectively, connected each other in the  $\Gamma$ -M direction and form a nodal chain structure. Our finding is remarkably distinguished from the nodal chain discussed in Ref. [1], where nonsymmorphic space group with glide plane symmetry are necessary. In our paper, the finding nodal chain is protected by mirror symmetry, which may happen in simple space group for spinless system. This property makes it possible to design the nodal chain states in weak SOC electronic systems, photonic crystal systems, or phononic crystal systems. After taking the SOC into consideration, the nodal chain structure degenerates into 30 pairs of Weyl points. We study the surface states on the (001) and (100) surfaces and show the patterns for the Fermi arcs connecting the Weyl points with different Fermi energy.

*Acknowledgments.* The authors thank Chen Fang and Xi Dai for very helpful discussions. This work was supported by the National Natural Science Foundation of China (No.11422428, No.11674369, No.11404024 and No.11674077), the National Key Research and Development Program of China (No.2016YFA0300600), the 973 program of China (No.2013CB921700) and the Strategic Priority Research Program (B) of the Chinese Academy of Sciences (No.XDB07020100). R.Y. acknowledges funding from the National Thousand Young Talents Program. Q. W was supported by Microsoft Research and the Swiss National Science Foundation through the National Competence Centers in Research MARVEL and QSIT.

- 
- [1] T. Bzdusek, Q. Wu, A. Ruegg, M. Sigrist, and A. A. Soluyanov, *Nature* **538**, 75 (2016).
  - [2] H. Weng, X. Dai, and Z. Fang, *Journal of Physics: Condensed Matter* **28**, 303001 (2016).
  - [3] B. Bradlyn, J. Cano, Z. Wang, M. G. Vergniory, C. Felser, R. J. Cava, and B. A. Bernevig, *Science* **353** (2016).
  - [4] H. Weng, C. Fang, Z. Fang, and X. Dai, *Phys. Rev. B* **94**, 165201 (2016).
  - [5] Z. Zhu, G. W. Winkler, Q. Wu, J. Li, and A. A. Soluyanov, *Phys. Rev. X* **6**, 031003 (2016).

- [6] H. Weng, C. Fang, Z. Fang, and X. Dai, *Phys. Rev. B* **93**, 241202 (2016).
- [7] Z. Wang, Y. Sun, X.-Q. Chen, C. Franchini, G. Xu, H. Weng, X. Dai, and Z. Fang, *Phys. Rev. B* **85**, 195320 (2012).
- [8] Z. Wang, H. Weng, Q. Wu, X. Dai, and Z. Fang, *Phys. Rev. B* **88**, 125427 (2013).
- [9] B. J. Wieder, Y. Kim, A. M. Rappe, and C. L. Kane, *Phys. Rev. Lett.* **116**, 186402 (2016).
- [10] X. Wan, A. M. Turner, A. Vishwanath, and S. Y. Savrasov, *Phys. Rev. B* **83**, 205101 (2011).
- [11] G. Xu, H. Weng, Z. Wang, X. Dai, and Z. Fang, *Phys. Rev. Lett.* **107**, 186806 (2011).
- [12] H. Weng, C. Fang, Z. Fang, B. A. Bernevig, and X. Dai, *Phys. Rev. X* **5**, 011029 (2015).
- [13] S.-Y. Xu, N. Alidoust, I. Belopolski, Z. Yuan, G. Bian, T.-R. Chang, H. Zheng, V. N. Strocov, D. S. Sanchez, G. Chang, C. Zhang, D. Mou, Y. Wu, L. Huang, C.-C. Lee, S.-M. Huang, B. Wang, A. Bansil, H.-T. Jeng, T. Neupert, A. Kaminski, H. Lin, S. Jia, and M. Zahid Hasan, *Nature Physics* **11**, 748 (2015).
- [14] A. A. Soluyanov, D. Gresch, Z. Wang, Q. Wu, M. Troyer, X. Dai, and B. A. Bernevig, *Nature* **527**, 498 (2015).
- [15] G. P. Mikitik and Y. V. Sharlai, *Phys. Rev. B* **73**, 235112 (2006).
- [16] A. A. Burkov, M. D. Hook, and L. Balents, *Phys. Rev. B* **84**, 235126 (2011).
- [17] M. Phillips and V. Aji, *Phys. Rev. B* **90**, 115111 (2014).
- [18] C.-K. Chiu and A. P. Schnyder, *Phys. Rev. B* **90**, 205136 (2014).
- [19] G. Bian, T.-R. Chang, R. Sankar, S.-Y. Xu, H. Zheng, T. Neupert, C.-K. Chiu, S.-M. Huang, G. Chang, I. Belopolski, D. S. Sanchez, M. Neupane, N. Alidoust, C. Liu, B. Wang, C.-C. Lee, H.-T. Jeng, C. Zhang, Z. Yuan, S. Jia, A. Bansil, F. Chou, H. Lin, and M. Z. Hasan, *Nature Communications* **7**, 10556 (2016).
- [20] R. Li, H. Ma, X. Cheng, S. Wang, D. Li, Z. Zhang, Y. Li, and X.-Q. Chen, *Phys. Rev. Lett.* **117**, 096401 (2016).
- [21] C. Fang, H. Weng, X. Dai, and Z. Fang, *Chinese Physics B* **25**, 117106 (2016).
- [22] H. Weng, Y. Liang, Q. Xu, R. Yu, Z. Fang, X. Dai, and Y. Kawazoe, *Phys. Rev. B* **92**, 045108 (2015).
- [23] Y. Kim, B. J. Wieder, C. L. Kane, and A. M. Rappe, *Phys. Rev. Lett.* **115**, 036806 (2015).
- [24] R. Yu, H. Weng, Z. Fang, X. Dai, and X. Hu, *Phys. Rev. Lett.* **115**, 036807 (2015).
- [25] C. Fang, Y. Chen, H.-Y. Kee, and L. Fu, *Phys. Rev. B* **92**, 081201 (2015).
- [26] P. Hosur and X. Qi, *Comptes Rendus Physique* **14**, 857 (2013).

- [27] D. T. Son and B. Z. Spivak, *Phys. Rev. B* **88**, 104412 (2013).
- [28] X. Huang, L. Zhao, Y. Long, P. Wang, D. Chen, Z. Yang, H. Liang, M. Xue, H. Weng, Z. Fang, X. Dai, and G. Chen, *Phys. Rev. X* **5**, 031023 (2015).
- [29] T. T. Heikkilä, N. B. Kopnin, and G. E. Volovik, *JETP Letters* **94**, 233 (2011).
- [30] J. Yang and F. Gao, *Physica Status Solidi (b)* **247**, 2161 (2010).
- [31] G. Kresse and J. Furthmüller, *Phys. Rev. B* **54**, 11169 (1996).
- [32] J. P. Perdew, K. Burke, and M. Ernzerhof, *Phys. Rev. Lett.* **77**, 3865 (1996).
- [33] P. E. Blöchl, *Phys. Rev. B* **50**, 17953 (1994).
- [34] M. P. L. Sancho, J. M. L. Sancho, J. M. L. Sancho, and J. Rubio, *Journal of Physics F: Metal Physics* **15**, 851 (1985).
- [35] N. Marzari, A. A. Mostofi, J. R. Yates, I. Souza, and D. Vanderbilt, *Rev. Mod. Phys.* **84**, 1419 (2012).